Oscillatory Behavior during the Catalytic Partial Oxidation of Methane: Following Dynamic Structural Changes of Palladium Using the QEXAFS Technique

Stoetzel, Jan; Frahm, Ronald; Kimmerle, Bertram; Nachtegaal, Maarten; Grunwaldt, Jan-Dierk

Published in:
Journal of Physical Chemistry Part C: Nanomaterials and Interfaces

Link to article, DOI:
10.1021/jp2052294

Publication date:
2012

Document Version
Publisher's PDF, also known as Version of record

THE JOURNAL OF PHYSICAL CHEMISTRY C

ARTICLE

pubs.acs.org/JPCC

Oscillatory Behavior during the Catalytic Partial Oxidation of Methane: Following Dynamic Structural Changes of Palladium Using the QEXAFS Technique

Jan Stötzel,[*,†] Ronald Frahm,[†] Bertram Kimmerle,[‡] Maarten Nachtegaal,[§] and Jan-Dierk Grunwaldt[*,∥,⊥]

[†]Fachbereich C—Physik, Bergische Universität Wuppertal, Gaussstr. 20, D-42097 Wuppertal, Germany

[‡]Gutenbergstr. 35, CH-3011 Bern, Switzerland

[§]Paul-Scherrer-Institut (PSI), CH-5232 Villigen, Switzerland

[∥]Institute for Chemical Technology and Polymer Chemistry, Karlsruhe Institute of Technology (KIT), Kaiserstr. 12, D-76128 Karlsruhe, Germany

[⊥]Department of Chemical and Biochemical Engineering, Technical University of Denmark, Building 229, DK-2800 Kgs. Lyngby, Denmark

Supporting Information

ABSTRACT: Pd/Al_2O_3 catalysts oscillate between ignition and extinction of the catalytic partial oxidation of methane when they are exposed to a 2:1 reaction mixture of methane and oxygen. The oscillations of the catalytic performance and the structure of Pd/Al_2O_3 catalysts in a fixed-bed reactor were investigated using spatially and time-resolved in situ quick scanning X-ray absorption spectroscopy with online mass spectrometry. The dynamic methane conversion oscillated between an inactive state, where only combustion occurred, and an active state, after ignition, where partial oxidation of methane as a combination of total oxidation and reforming in the catalytic capillary reactor was observed. This change in catalytic performance was directly linked to changes in the oxidation state of the Pd/Al_2O_3 catalysts at different positions along the catalytic reactor. During the ignition of the catalytic partial oxidation of methane, the catalyst reduced from the end to the beginning of the catalyst bed and oxidized again toward the end as soon as the entire catalyst bed was reduced. On an entirely oxidized catalyst bed, only total oxidation of methane was observed and consumed the oxygen until the conditions at the end of the catalyst bed lead to a reduction of the catalyst bed again and a new cycle began with partial oxidation. Prior to the oxidation of the catalyst, a temporary lattice expansion appeared, which could be assigned to carbon intercalation into the palladium lattice. Furthermore, a sintering of the Pd particles at increasing age of the catalyst was observed, which leads to a lower oscillation frequency. Effects of particle size, oven temperature, and oxygen/methane ratio on the oscillation behavior were studied in detail. The deactivation period (reoxidation of Pd) was much less influenced by the oven temperature than the ignition behavior of the catalytic partial oxidation of methane. This indicates that deactivation is caused by an autoreduction of the palladium at the beginning of the catalyst bed due to the high temperature achieved by total oxidation of methane.

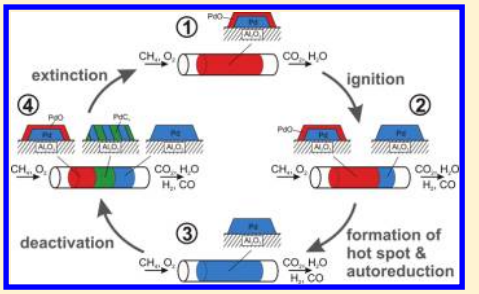

1. INTRODUCTION

Kinetic oscillations during heterogeneous catalytic processes are a well-known and well-studied effect, which is observable on single-crystal surfaces as well as on industrially relevant supported particles with diameters of a few nanometers.[1−7] Many theoretical models to describe such oscillations were developed in the past and refined several times during the last three decades. In theoretical approaches, oscillations are suggested to appear in narrow ranges of reactant gas pressure, which correspond to bistable regions close to the transition lines in surface phase diagrams, as can, for example, be calculated with density functional theory.[8] This was confirmed experimentally and width of such bistable regions was observed as hysteresis in the rate of conversion depending on the direction of changes in reactant pressure.[9,10] Within the bistable regions, an additional, relatively slow process is determining the temporal character of the oscillations, which is suggested to be adsorbate-induced surface restructuring,[11] oxide formation,[12] or carbon deposition,[13] as also summarized by Zhdanov.[9] Recently, it was shown that the regions of bistability become smaller with an increasing number of defects, such as steps and edges, so that oscillations and chaotic phenomena are pronounced in the case of very small particles.[10] Moreover, it was shown that smoothing and roughening of the catalytically active surface have to be considered as decisive parameters for kinetic oscillations.[14]

Received: June 3, 2011
Revised: October 19, 2011
Published: November 07, 2011

Although there are many studies about kinetic oscillations in catalysis, most theoretical and experimental approaches, as, for example, all the ones that are referred to above, were performed for the important catalytic reactions that deal with the oxidation of CO and NO. Many ideas can be adapted to the catalytic partial oxidation of methane, but most of them depend on the specific properties of the appearing absorbents, which makes it difficult to generalize them for other catalytic experiments. Moreover, many experimental studies were carried out under idealized conditions, while nonlinear terms can play a role in macroscopic systems, such as catalytic reactors, where, for example, temperature or concentration gradients appear. Real working catalysts and conditions imply supported particles with a diameter of a few nanometers in gas streams at normal or elevated pressure and elevated temperatures.[15−21] This drastically reduces the number of feasible characterization tools, since most of them require either vacuum conditions, for example, for electron detection, or long-range lattice orders, for example, for diffraction techniques. Here, X-ray absorption spectroscopy (XAS) has proven to be an invaluable approach for such systems.[16,20−28] The extended X-ray absorption fine structure (EXAFS) region yields information on the local order (up to ∼6 Å) of the catalytically active species. Because the oscillations are a dynamic process, typically on the second scale, only time-resolved EXAFS techniques are usable here. These have been previously used to study oscillations, for example, during the oxidation of CO on Pd,[29] during the partial oxidation of methane over supported Pd-particles,[30] and, more recently, during the extinction of CO conversion on a Pt catalyst used for CO oxidation.[31] We will apply the quick-scanning EXAFS (QEXAFS) technique[32,33] to study stable oscillations on a Pd/Al_2O_3 catalyst during catalytic partial oxidation (CPO) of methane. The QEXAFS technique in combination with spectra averaging has recently proven to yield good data quality for EXAFS analysis in experiments with the same 5 wt % Pd/Al_2O_3 catalyst as used in the present work.[34]

As an alternative to steam reforming, the CPO of methane is of interest to the gasoline-producing industry to make use of residual methane appearing, for example, during oil production, and also for mobile applications, such as the on-board generation of synthesis gas for fuel-cell-driven cars.[36,37] The overall reaction scheme for the CPO of methane is

$$CH_4 + 0.5O_2 \leftrightarrow CO + 2H_2;\ \Delta H^0 = -35.9\ \text{kJ mol}^{-1}$$

Oscillatory behavior during methane combustion was observed on a variety of transition-metal catalysts[38,39] besides Pd, which is the one investigated here. One of the first reports on oscillations during the oxidation of methane on Pd was published by König et al.[40] Since then, several studies of kinetic oscillations during the oxidation of methane were carried out.[41−46] However, few of these were based on supported catalysts and none of them used QEXAFS as an in situ technique to resolve the structure of the catalyst at different stages during the oscillations.

An important conclusion of our recent study, where we combined XAS, IR thermography, and mass spectroscopy (MS), was that the structure of the catalyst depends on both the time during one oscillation period and the position in the reactor.[30] In this previous study, only integral structural information was obtained. Hence, here, the QEXAFS technique with a ca. 100−200 μm horizontal spatial resolution was used to provide structural information as a function of time and as a function of position in the reactor. A large parameter space was taken into account to investigate the effect of temperature, aging, gas flow, and gas composition on the oscillations.

2. EXPERIMENTAL METHODS

2.1. Catalyst Samples and Catalytic Experiments. Two different Pd catalysts were used. A commercial 5 wt % Pd/Al_2O_3 (Johnson Matthey 324; mean particle size of 3.4 nm; as determined by TEM) and a 5 wt % Pd/Al_2O_3 catalyst that was prepared by flame spray pyrolysis (denoted FSP catalyst). The particle size of the FSP catalyst on similar samples was determined to be 2−4 nm with TEM. To prepare the FSP catalyst, first, a solution of Pd(II) acetylacetonate (purum, Fluka) and Al(III) acetylacetonate (99%, ABCR) in a freshly mixed solution of 50/50 (v/v) methanol and, second, acetic acid was sprayed into a methane oxygen flame via a nozzle.[47,48] In each case, 40 mL of the corresponding solution was fed by a syringe pump (Inotech, 50 mL syringe, 3 mL min^{-1}) into the center of a methane/oxygen flame ring. Approximately 50 cm above the flame, a steel vessel containing a cylindrical filter was mounted. Product particles were collected on a glass fiber filter (Whatman GF/A, 26 cm in diameter) with the help of a vacuum pump. The inner 22 cm of the filter was scraped off using a spatula. The powder was pressed, crushed, and sieved to fractions between 100 and 200 μm for the spectroscopic/catalytic experiments. The catalysts were then loaded as a fixed bed (about 5 mg) in a quartz capillary (Markröhrchen, Hilgenberg GmbH, 1 mm diameter, wall thickness of 20 μm) with a gas inlet and outlet. The reactor was mounted on a gas blower, which provided heating of the sample. The setup has been described in more detail in ref 26. The reaction mixture for most of the reported experiments was 3% O_2/6% CH_4/He, excluding the series of measurements with varying gas mixtures, as referred to further below. Flow rates were adjusted by mass flow controllers (Brooks) and checked at the outlet of the reactor before the experiment by a gas flow meter (7-gas flow meter, Raczek). The sample temperature was measured just below the capillary via a thermocouple. The capillary reactor was connected to a mass spectrometer for online gas analysis (Balzers Thermostar).

2.2. QEXAFS Measurements. All QEXAFS measurements were performed at the SuperXAS beamline[49] of the Swiss Light Source (SLS, Villigen, Switzerland). The polychromatic radiation of the 2.9 T supercooled bending magnet was collimated with a Pt-coated mirror before it was monochromatized by double reflection from a Si(311) channel-cut crystal. The crystal was mounted on the oscillating tilt table inside the QEXAFS monochromator working with excenter mechanics.[50] A crystal oscillation frequency of 1 Hz yielded continuously two spectra each second collected at the Pd K edge, one with increasing energy, followed by the decreasing scan to the start energy. The fixed excenter disk installed in the QEXAFS mechanics yielded an energy range from 24.19 to 26.02 keV for each spectrum. A second Pt-coated toroidal mirror was used to focus the beam onto the capillary with the catalyst located between two ionization chambers each 15 cm in length. The first chamber was filled with Ar, the second with Kr, both at ambient pressure and with 1.5 kV connected to the chamber plates mounted with a gap of 10 mm. An additional long ionization chamber (30 cm) filled with argon was used to measure a Pd metal foil behind the second chamber simultaneously with the sample to get an absolute calibration point for the energy scale of the sample spectra. To get accurate energy values relative to this point, the angle of the

crystal inside the QEXAFS monochromator was measured simultaneously with each absorption value using a fast angular encoder.[51,52]

2.3. Data Analysis. The rather extended range of about 2 keV of the QEXAFS spectra yielded moderate photon statistics and had to be compensated for by averaging/smoothing procedures over several spectra, which leads to a reduced effective time resolution. Averaging over five spectra proved to be sufficient to study most effects of interest. More advanced techniques had to be applied to achieve a better signal-to-noise ratio while maintaining a reasonable time resolution, which is explained below. Data analysis was carried out with homemade software mainly based on scripting and the IFEFFIT code.[53] With E_0 fixed at 24.355 keV, the pre- and postedge were fitted before the $\chi(k)$ was extracted via the AUTOBK algorithm and k^3-weighted. Thereafter, FEFF6 was used to calculate phase and amplitude functions of the different scattering paths[54] as required for the EXAFS analysis, which was typically carried out within a Kaiser-Bessel window in k-space from 1.6 to 11.9 $Å^{-1}$ and within a Kaiser-Bessel window in R-space from 1.2 to 3.2 Å. The S_0^2 reduction factor required to calculate the exact coordination numbers was determined to be 0.81(5) by fitting the first shell of the Pd metal foil spectra measured as a reference, where the nearest-neighbor coordination number is set to 12 for the fcc structure. For the linear combination analysis (LCA), which was also carried out with the IFEFFIT code, the spectra were normalized and fitted within the near-edge range of 24.325−24.405 keV with reference spectra that were normalized in the same way. The E_0 was kept fixed for the LCA, and the resulting weights were forced to sum up to 100%. To find the number of statistically significant independent components, a principal component analysis (PCA) was performed. As a pure mathematical approach to reveal correlations in the data, the PCA, in contrast to the LCA, does not rely on references. Two factor retention decision criteria were applied to the PCA results. The first was to compare the results to the ones of a second PCA, performed on a data matrix of the same dimension as the one including the measured data, but instead filled with random noise (parallel analysis).[55] The second one is achieved by fitting the tail of the sorted eigenvalues and considering only the first values that lie above this fit as significant (scree plot).[56]

3. RESULTS AND DISCUSSION

3.1. QEXAFS Data during Chemical Oscillations. The oscillations of the two Pd/Al_2O_3 catalysts were studied under various reaction conditions, including the age of the catalyst in the gas stream, temperature, and gas composition. Figure 1 shows a series of QEXAFS spectra of the 5 wt % $PdAl_2O_3$ catalyst prepared by flame spray pyrolysis (FSP) during typical chemical oscillations at 410 °C and a gas flow of 27 mL/min; each spectrum set is the result of averaging over five spectra. The normalized measuring position was with $x/L = 0.93$ rather at the end of the catalyst bed with the absolute length $L = 7.5$ mm. The X-ray absorption near-edge structure (XANES) region shows that two different states (one reduced and one oxidized state) are clearly distinguishable during the oscillations. Obviously, these two states are rather stable apart from the periodic transitions between them, which proceed much faster. To verify these observations quantitatively and to compare runs with different settings, an LCA (linear combination analysis) with spectra of metallic palladium and palladium oxide was performed to determine the relative

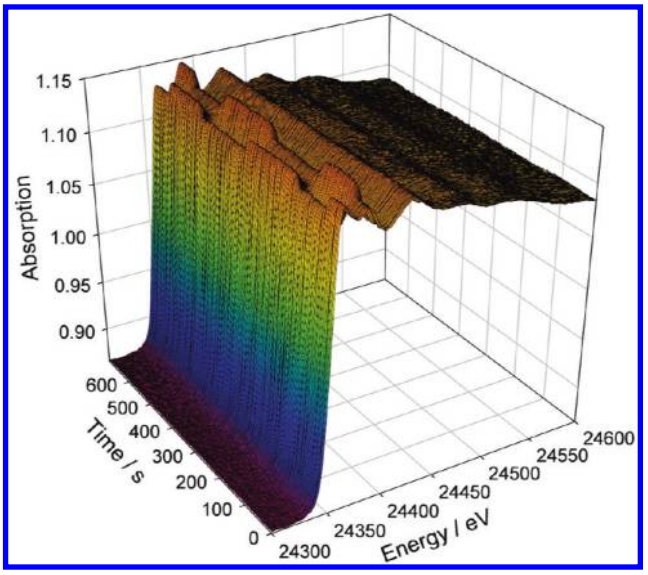

Figure 1. Change of the QEXAFS spectra measured at the Pd K edge during the oscillations. These spectra were measured with the FSP catalyst at the end of the fixed catalyst bed ($x/L = 0.93$) at 410 °C and 27 mL/min of 6% CH_4/3% O_2/He.

amount of oxidized and reduced Pd during the oscillations. In Figure 2a spectra of both stable states, observed during the oscillations (Figure 1), are shown together with LCA fits. Although the structure of the XANES is generally well reproduced by the fits, certain deviations appear due to the nanosized character of the investigated catalysts compared to the large particle references, resulting in less significant scattering features. Additionally, the differences in temperature are contributing to the deviations. Thus, the LCA results have to be handled with care concerning the quantitative values, which was also discussed by Iglesias-Juez et al.[57] within a time-resolved EXAFS study of Pd/Al_2O_3 nanosized particles. Accordingly, further EXAFS analysis is required to resolve the structure of the oxidized and reduced Pd more accurately, which will be discussed in section 3.4. Here, the LCA results are a reasonable approach to characterize the oscillations, as they reveal the temporal character of the oscillations and also the relative changes in the amounts of the used references during the performed runs with different parameter settings. With the results of the commercial catalyst shown in Figure 2b, a slightly stronger contribution of metallic Pd can be observed in both investigated states, which is significant with respect to the achieved data quality. However, the difference to the FSP catalyst is more enhanced in the oxidized state. This can be linked to the fact that the FSP catalyst is highly dispersed over the support and thus provides smaller particles. This directly results in a higher PdO/Pd ratio in the oxidized state according to the higher surface/volume ratio.

3.2. Systematic LCA Analysis of the QEXAFS Data in Comparison to Online Gas Analysis. LCA analysis was performed for all spectra of each parameter set. This allows investigating and comparing the oscillations in more detail at different positions along the capillary as shown in Figure 3, where the mass spectrometry signals of H_2 and O_2 are displayed as well. First of all, this figure shows that oscillations in catalytic activity and between reduced and oxidized Pd occur simultaneously, while the qualitative impression that the two states of the oscillation are rather stable, as qualitatively deduced from Figure 1, is confirmed.

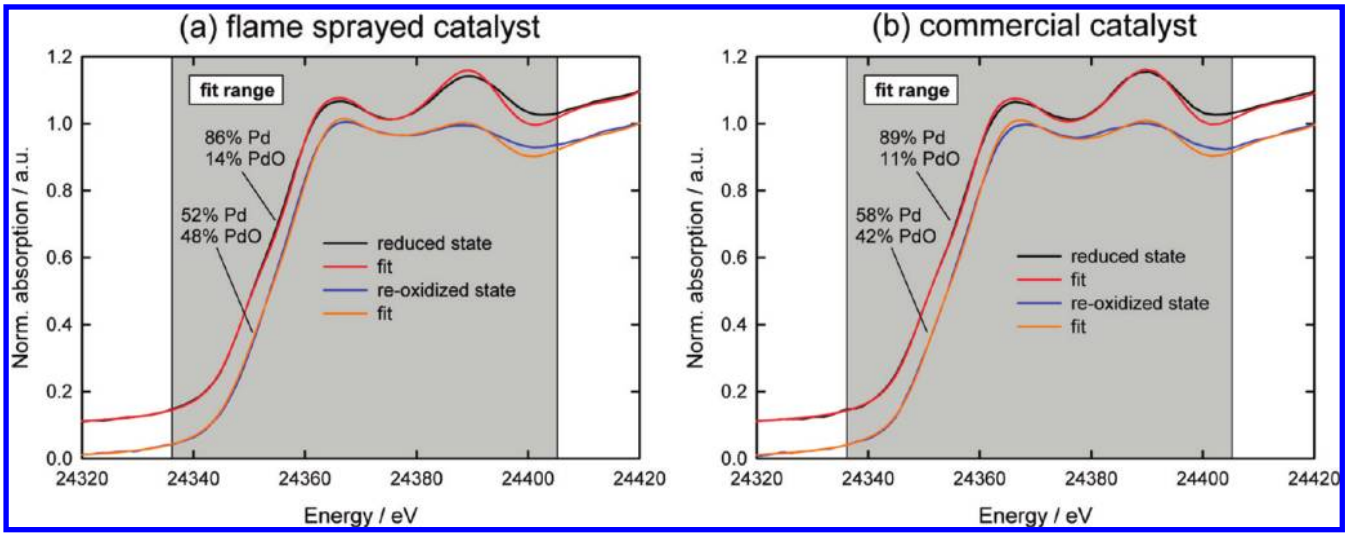

Figure 2. LCA results of two XANES spectra representing the two different Pd states appearing during the oscillations: (a) FSP catalyst from the same measurement as in Figure 1 and (b) the commercial catalyst again at the end of the capillary with the same flow of 27 mL/min of 6% CH_4/3% O_2/He, but at 385 °C.

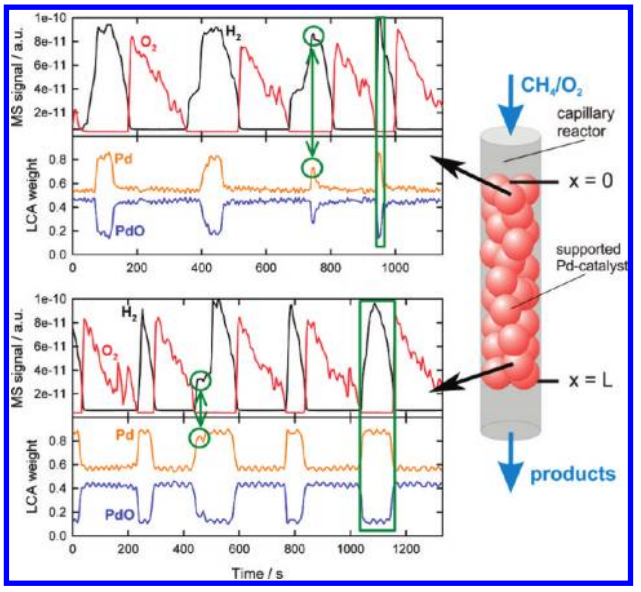

Figure 3. Results of systematic LCA in comparison to the MS signal for observed oscillations at the beginning and the end of the catalytic fixed bed (upper part, $x/L = 0$; lower part, $x/L = 1$). Both of these experiments were performed for the FSP catalyst at 410 °C in a 27 mL/min flow of 6% CH_4/3% O_2/He. The green boxes show the correspondence of the duration of hydrogen production and the catalyst being in the reduced state at the respective position. The green circles display the close correlation of chemical reaction and Pd oxidation state with the help of unique features.

Furthermore, the reduced state lasts much longer at the end of the catalyst bed, suggesting that a reduction front moves from the end of the capillary to the beginning and, afterwards, back to the end again.[30,58] This behavior and its correlation with the observation that hydrogen is only produced when part of the catalyst bed is in a reduced state has been shown before for the ignition of CPO on Rh and Pt catalysts and for the oscillative CPO on a Pd catalyst.[30,35,59] The green boxes in Figure 3 show that the duration of hydrogen production corresponds to the time, during which the catalyst stays in the more reduced state at position $x/L = 1$. In contrast to that, at $x/L = 0$, the duration of hydrogen production lasts always significantly longer than the reduced state of the catalyst. The green circles, on the other hand, mark unique features in the LCA and MS data that proceed simultaneously and demonstrate the close relation between the oxidation state of the sample and the gaseous products.

The illustration in Figure 4 demonstrates how the oscillations propagate through the catalyst bed and how different states of the catalyst influence the oscillatory behavior. When H_2 was detected at the outlet of the catalyst, the catalyst was considered as active (red curve). As long as the LCA weight of oxidized Pd was equal or higher than 30% at the specified position of the catalyst bed, the catalyst was considered as oxidized at this position. With this simplification, data of runs with different temperatures and different aging times of the catalyst can be compared. As assumed in previous studies,[48,59,60] we observed that palladium starts to reduce at the end of the catalyst bed as soon as the partial oxidation of methane starts. Afterward, the reduction process moves upstream along the catalyst bed until the amount of produced H_2 is at a maximum (cf. Figure 3). At this point, Pd oxidizes again toward the end of the capillary until finally the entire catalyst is "inactive" again; that is, only total oxidation is present. In addition, the reduction process (ignition of partial oxidation) moves slightly faster along the catalyst bed than the oxidation process (extinction). This can be seen, for instance, when looking at the position close to $x = 0$ for the catalyst at 418 °C. Here, in most oscillations, the catalyst is reduced shortly after the first H_2 is detected, while the catalyst stays significantly longer oxidized, at this position, before the H_2 production disappears again. This is in agreement with IR thermography results[30] and also CPO over Rh-based catalysts, where the ignition is faster than the reoxidation.[35] Under certain conditions (for instance, 418 °C, 26 mL/min of 6% CH_4/O_2/He), it has been observed that there are oscillations superimposed on the actual CPO oscillation in structure, as shown in Figure 5, where the hydrogen partial pressure does not go back to zero. The oxidation state of the Pd at the entrance of the catalyst bed is synchronous to the MS signal, since both show—within the margin of error—exactly the same features. A similar effect was

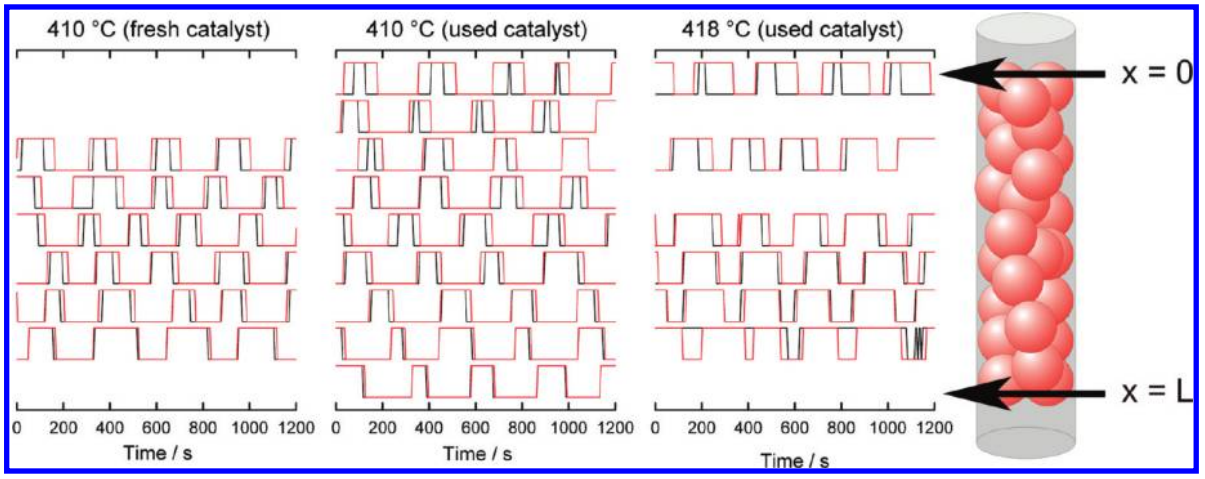

Figure 4. Overall activation state of the catalyst (red curve) and the reduction state at certain positions along the capillary (black curve) are plotted for experiments with the flame-sprayed catalyst carried out under different conditions with a flow of 27 mL/min. The red curve on the "high" level means that H_2 is produced, and a low level means no hydrogen production. For the black curve, "high" means that the catalyst is reduced at this position along the catalyst bed. The position is plotted along the capillary, as sketched on the right side.

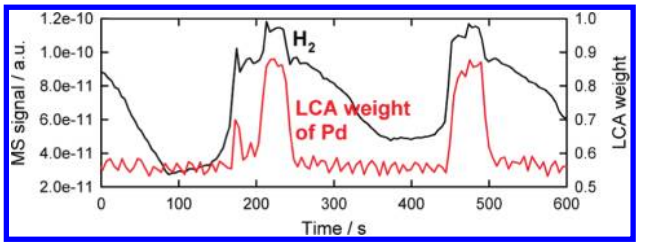

Figure 5. Inner oscillation (superimposed on the actual oscillation of CPO) in hydrogen production and oxidation state of the Pd catalyst at the beginning of the catalyst bed (x/L = 0). Conditions for the FSP catalyst in this case were 418 °C and 27 mL/min of 6% CH_4/3% O_2/He.

observed in a previous study on a Rh catalyst, dealing with CPO under non-oscillating conditions.[61]

By combining the findings from Figures 3 and 4, a first explanation of the oscillations is possible, which supports earlier findings.[30] In the oxidized state of the catalyst, surplus oxygen is increasingly consumed by the total oxidation of methane until no more oxygen reaches the end of the catalyst bed. The catalyst starts to reduce from the end of the catalyst bed upstream, and the CPO starts at the same instance. That is, hydrogen is produced. As soon as the entire catalyst bed is reduced, an oxidation front moves downstream and oxidizes the Pd again from the beginning to the end of the catalyst bed. The amount of oxygen detected by MS reaches a maximum and immediately starts to decrease, indicating the start of a new cycle. On the basis of previous IR thermography results,[30] the described behavior can be refined in the following way: While the catalyst is still in its oxidized state, a hotspot forms in the first half of the catalyst bed. At the position of the hotspot, more and more oxygen is consumed. When the oxygen consumption reaches 100%, hydrogen starts to be formed and a reduction front moves through the catalyst bed. The oxidized zone on the inlet side of the reactor, in which all oxygen still has to be consumed, becomes more and more contracted, which raises the local temperature.[30] At a certain point, the temperature is high enough to cause self-reduction[62] of the still-oxidized Pd. Thereby, the relevant species switches from oxidized to reduced Pd, which is less active for total oxidation of methane. The heat production becomes insufficient for hydrogen

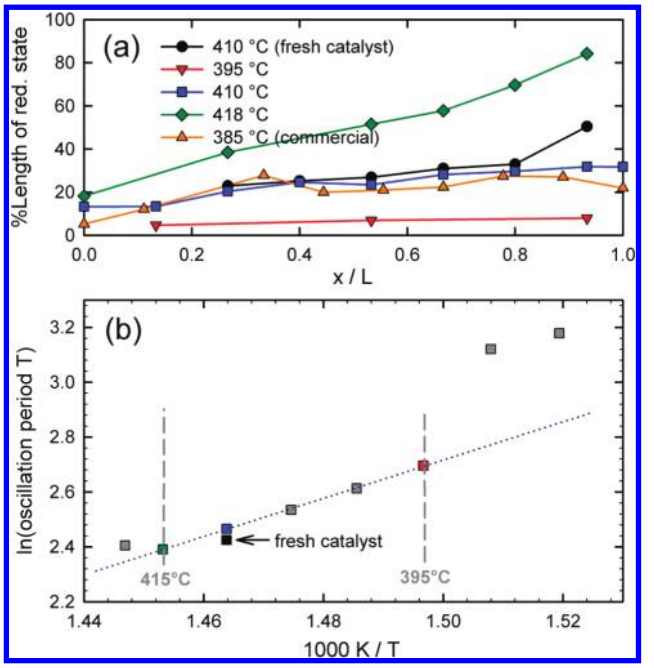

Figure 6. (a) The average percentage in time of an oscillation period where the catalyst is in the reduced state as a function of the position within the capillary and for different temperatures. (b) The logarithm of the oscillation period versus the reciprocal value of the temperature with a linear fit in the temperature range where the oscillations are stable. All measurements were performed with a flow of 27 mL/min of 6% CH_4/3% O_2/He.

production, and the local temperature is lowered enough for the reoxidation of the catalyst bed. This is an indirect proof of the combustion−reforming mechanism also shown on other noble metal catalysts.[63,64]

3.3. Frequency of Oscillations and Relative Width of the Reduced State. With the LCA results, the relative width of the reduced state for each measurement at variable positions along the catalyst and also for variable temperatures can be determined. Additionally, the MS signal of, for example, H_2 can be used to determine the frequency of the oscillations. Both are displayed in Figure 6a,b.

dx.doi.org/10.1021/jp2052294 |J. Phys. Chem. C 2012, 116, 599–609

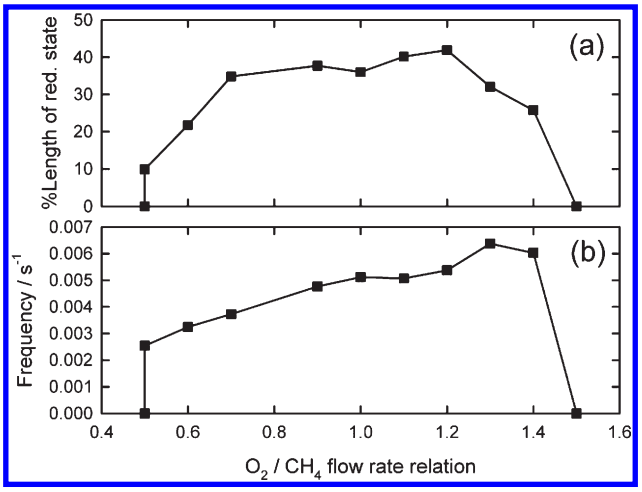

Figure 7. (a) Duration of the reduced state in one oscillation cycle, that is, the average percentage in time of an oscillation period where the catalyst is in the reduced state as a function of the inlet gas composition. (b) Frequency of the oscillations as a function of the O_2/CH_4 ratio. The FSP catalyst was used with a fixed temperature of 418 °C and measured at the relative position x/L = 0.67.

The black, red, blue, and green graphs in Figure 6a are measured with the same FSP catalyst, whereas the yellow one represents the results for the commercial catalyst. All measurements were performed with the same flow of 26 mL/min of 6% CH_4/3% O_2/He. For reaction kinetic reasons, the relative length of the reduced state of the oscillation is longer at higher temperatures. The width of the reduced state varies stronger along the catalyst bed at higher temperatures. At 385 °C, the commercial catalyst shows a similar relative length of the reduced form as the FSP catalyst at 410 °C. Figure 6b shows that the frequency of the oscillations increases with temperature to a maximum of about 0.004 s^{-1} at about 415 °C/418 °C. At more than about 420 °C, the catalyst stops to oscillate, and below about 385 °C, no ignition occurs. Between 395 and 415 °C, the oscillations are stable and reproducible. In this region, Zhang et al. have interpreted the temperature dependence of the oscillations in terms of activation energy.[44] Similarly, it can be observed in Figure 6b that the duration of the oscillation period follows an Arrhenius-type function, as shown by the linear fit, which yields a corresponding activation energy for the oscillation of E_a = 58 kJ mol^{-1}. Slightly higher activation energies of at least 68 kJ mol^{-1} were found for oscillations on Pd metal foils and wires.[44] Here, the temperature is measured below the catalyst bed, and the temperature in the fixed bed can locally be significantly higher.[30] The fresh catalyst at 410 °C oscillates somewhat faster than the aged catalyst at the same temperature (see Figure 6b). This can be assigned to the smaller particle size (see section 3.4) and leads to a higher reaction rate at lower temperature, and thus probably faster autoreduction. The commercial catalyst oscillates at a higher frequency between 0.005 and 0.006 s^{-1}, but the values scatter strongly, indicating less-stable oscillations for this catalyst. The higher oscillation frequency may be linked to the fact that the density of the FSP-made catalyst is lower and thus less Pd is present in the capillary.

The relative width of the reduced state and the frequency of the oscillation are displayed as a function of variable O_2/CH_4 flow ratios in Figure 7. The temperature was held at 400 °C, and data were recorded at a fixed position of x/L = 0.67. At an O_2/CH_4 ratio of 0.5, the measurement was repeated. At the chosen temperature and a total flow of 27 mL/min, no oscillations are observable for O_2/CH_4 ratios lower than 0.5 or higher than 1.5. The graph representing the relative duration of the reduced state is very symmetric around a flow rate relation of 1.0, and the relative length of the reduced state during the oscillations is very stable at about 40% with O_2/CH_4 ratios ranging between 0.7 and 1.3. However, the frequency of the oscillations increases linearly with the O_2/CH_4 ratio from about 0.0025 s^{-1} at 0.5 to about 0.006 s^{-1} at 1.4, whereas it is zero beyond these values. This demonstrates the influence of the exothermic reaction where a higher oxygen-to-methane ratio leads to a larger and faster hot spot evolution in the first part of the catalyst bed until the temperature is so high that even here the rate of total oxidation of metallic Pd is too large.

3.4. Shedding Light on the Structure of the Supported Palladium Particles by QEXAFS. To answer what the reduced and oxidized states really mean in terms of atomic structure, the Fourier transformed EXAFS data and fitting results for spectra of the two different states during the oscillations (Figure 1) are shown in Figure 8. The extracted EXAFS function $\chi(k)$ leading to these and to all further EXAFS results are presented in Figure S1 in the Supporting Information. The reduced state (black curve) is best fitted with only one Pd shell of bulk Pd metal. Additional oxygen or carbon shells did not significantly improve the fit for the chosen first shell R range up to 3 Å. This leads to the conclusion that reduced Pd nanoparticles are the dominant species during this state of the oscillation. The more oxidized state (blue curve) can be fitted with a Pd−O scattering path typical for PdO, and an additional Pd−Pd path. Here, the ratio of oxygen to palladium neighbors is lower than that expected for bulk PdO, which is due to the fact that only the surface of the Pd particles is oxidized. With respect to the EXAFS results, it can be calculated that about 82% of the particles are still reduced. Considering most densely packed particles with sizes of about 2−3 nm, as determined below, truncated cuboctahedrons built up with few hundred atoms are a realistic model. A maximum of only about 40−50% of all atoms in these particles would not be surface atoms.[70] According to the 82% reduced Pd, it can be concluded that only surface atoms are oxidized here. The fit results for the next Pd neighbors of the commercial catalyst (same data set as for Figure 2b) are displayed in Figure 8b and show good qualitative agreement with the results depicted in Figure 2b, since the structural parameters indicate a stronger bulk Pd character than for the FSP catalyst. In the oxidized state, still about 84% of the particle's volume is reduced. One can conclude from the LCA, PCA, and EXAFS evaluations so far that no further Pd-containing components seem to appear in significant amounts during the oscillations.[68] On the other hand, various adsorbates may be present that cause only minor changes in the EXAFS spectra.[29] Furthermore, PdC is a likely and suggested species[46] in the course of the oscillations and provides EXAFS features that resemble the first shell of bulk Pd.[69]

Under reducing conditions, the number of the next-neighboring Pd atoms can be further exploited to estimate the size of the particles. In Figure 9a, the average number of next Pd neighbors in the reduced state of the catalyst is plotted as a function of the position along the capillary for different aging stages of the catalyst. For the fresh catalyst, after 4 h in the gas stream, coordination numbers ranging from about 7.0 to about 7.5 can be observed. According to Jentys,[22] this corresponds to particles consisting of at least about 100 atoms considering densely packed cuboctahedrons, which results in a lower limit of ca. 2 nm for the particle sizes.[70] It has to be mentioned that the accurate particle shapes depend on the interaction between particles and the support

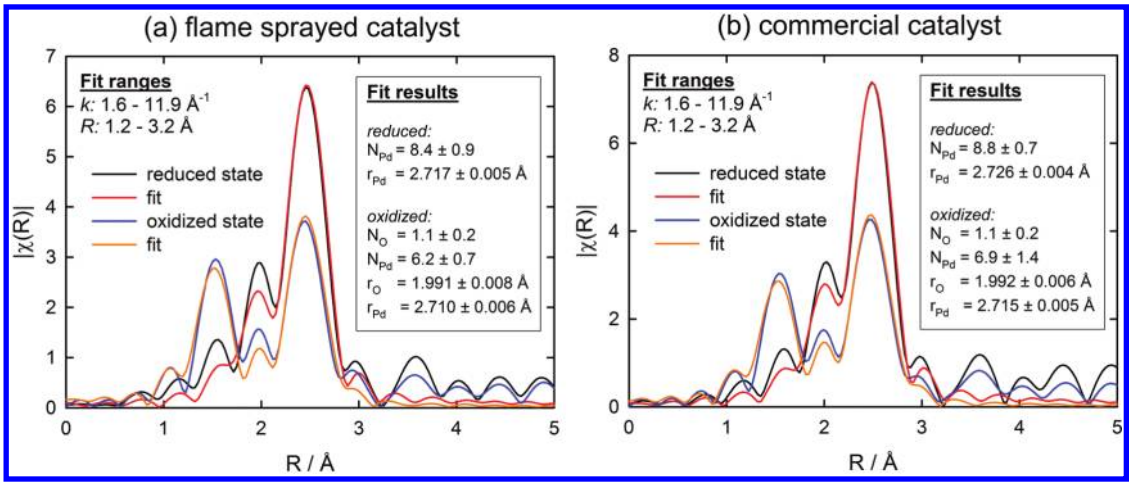

Figure 8. EXAFS fits of the oxidized and reduced states of the (a) FSP and (b) commercial catalyst, data from the measurement as shown in Figure 2. Averaging over all reduced and oxidized spectra of the data set was performed to obtain results as representative as possible for each state.

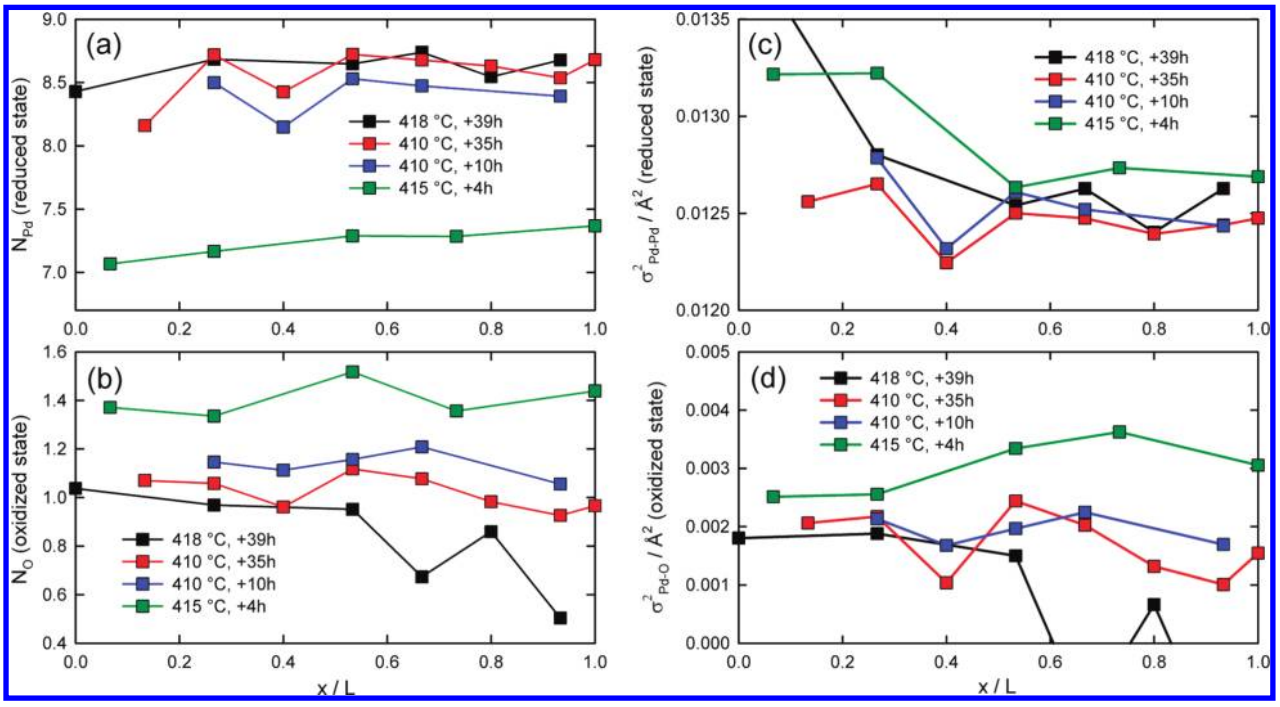

Figure 9. First shell coordination of Pd and first shell structural disorder in both states of the catalyst for different times on stream of the FSP catalyst and at different positions along the capillary: Number/disorder of next-neighbor (a)/(c) Pd atoms in the reduced state and (b)/(d) O atoms in the oxidized state. The time values are related to the very first reduction of the catalyst. A constant flow of 27 mL/min of 6% CH_4/3% O_2/He was fed over the catalyst during all experiments.

and also on the reactants so that distortions toward more slab-like shapes are not unlikely.[65−67] This would shift the ratio of inner atoms to surface atoms toward the latter ones, resulting in a lower integrated coordination number for the same number of contributing atoms[22] and accordingly an underestimation of particle sizes by our EXAFS analysis. After 10 h on stream, the number of next Pd neighbors increased to about 8.4 averaged over all positions and finally to an average value of about 8.7 after 39 h on stream, which corresponds to a minimum of about 150 atoms and about a 2−3 nm particle diameter considering cuboctahedrons (up to 900 atoms considering distorted cuboctahedrons or slabs[22]). Thus, the particle size of the catalyst increased during the experiments due to sintering. The typical uncertainty in the coordination numbers deduced from EXAFS first shell fits in fcc structures amounts to about 10%.[22] The uncertainty can be even higher for highly dispersed systems and high temperatures because significant anharmonic contributions to the Debye−Waller factor are expected to affect the low *k*-region of the EXAFS spectrum.[72] It was also revealed that Pd particle size determination by EXAFS generally tends to underestimate the particle sizes,[57] which can probably also be assigned to an anharmonic Debye−Waller factor due to enhanced disorder at the particle surface.[71] The relative error is rather low, as can be seen when comparing the results at different positions along the catalyst bed,

dx.doi.org/10.1021/jp2052294 |J. Phys. Chem. C 2012, 116, 599–609

which do not scatter that much. Thus, there is a systematic error of 10% or higher so that all the results in Figure 9 may actually have to be shifted up- or downward, but the qualitative observation of particle growth with the age of the catalyst is still valid. Comparison of the measurements after 10 h with the measurements after 35 h shows that the two curves have the same shape, except for the shift to a higher Pd coordination number. Sintering of Pd/Al_2O_3 catalysts in methane was suggested by Demoulin et al. (see ref 73), who heated the catalysts from room temperature to 550 °C and cooled them down to room temperature again. Afterward, they measured the CO chemisorption after a heat treatment of the samples at 400 °C in H_2 and measured XPS of the pressed catalyst. Probably, it is, in particular, the reduction to metallic palladium and the high exothermicity that leads to sintering,[62] although the reoxidation, in principle, could lead to a redispersion in each oscillation.

The increased particle size of the aged catalyst also affects the oscillation behavior, as can be observed in Figure 6 when comparing the black and the blue curves, which were measured under the same conditions. The relative duration of the active state is very similar. However, the fresher catalyst oscillates with a slightly higher frequency, which can be associated with the higher effective surface area of the smaller particles, which results in a higher catalytic activity and, therefore, a more rapidly evolving hot spot. From Figure 9b, it is clear that the average number of oxygen neighbors in the oxidized state of the oscillation decreases with larger particles. Only the outer surface of the Pd particles is oxidized so that the composition shifts to higher amounts of bulk Pd with larger particles.

The structural/thermal disorder can be taken into account by fitting the Debye−Waller factor during the EXAFS analysis. This is shown in Figure 9c,d for the first Pd shell of the reduced and the first oxygen shell of the oxidized catalyst. Disorder is highest at the beginning of the catalyst bed in the reduced state and decreases toward the end. This agrees well with the increased thermal disorder due to the evolving hot spot close to the beginning of the bed. The results look quite different for the oxidized state where the disorder does not vary that much. However, especially for the fresher catalysts, a maximum of the Debye−Waller factor is observable toward the end, in the region of $x/L = 0.6$ to $x/L = 0.8$. This is probably due to the fact that the catalyst heats up along the axial direction of the reactor due to the exothermic methane combustion that occurs over the whole catalyst bed.[30] At 418 °C, the oxidized phase at the end of the catalyst bed was too short-lived to achieve reasonable data quality for the EXAFS fits.

3.5. Analysis of Reduction and Reoxidation Behavior. The achieved time resolution and data quality are sufficient to analyze the structure not only averaged over the chemically stable conditions (partially oxidized and fully reduced) but also during the ignition and the extinction period.

A closer look at the LCA results for the oxidized state of the oscillations measured at the same position, but at different temperatures, is given in Figure 10. Figure 10a reveals that the oxidation proceeds similarly at all selected temperatures (395, 400, 405, and 410 °C) by means of an exponential $f(x) = A(1 - e^{-bx})$ increase of the PdO amount with a similar time constant for the first 60 s. Afterward, the amount of PdO increases to a maximum, which is already reached after about 60 s at 410 °C, whereas it takes about 240 s at 395 °C, thus yielding a higher amount of PdO. After half of the time, during which the catalyst is partially oxidized, the amount of PdO decreases linearly before the reduction occurs, as shown in Figure 10b. Linear fits, which are

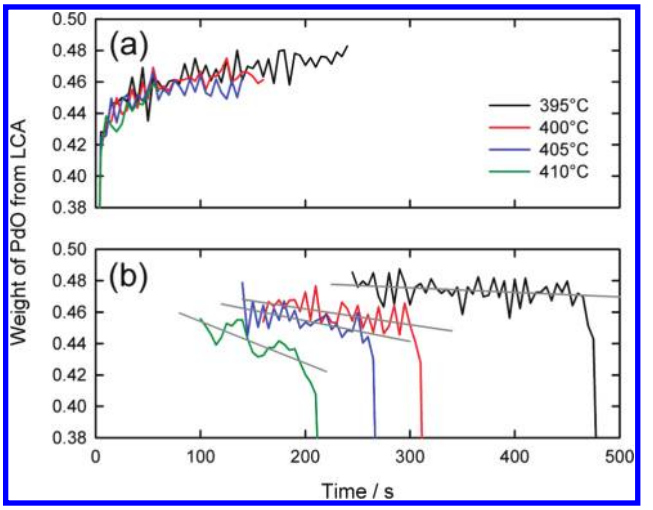

Figure 10. Amount of PdO calculated via LCA for the oxidized state of the catalyst at different temperatures (27 mL/min, 6% CH_4/3% O_2/He): (a) the first half of the oxidized state averaged over three oscillations and (b) the second half averaged over three oscillations.

added to the graph, show that the decrease of the PdO amount is significantly faster at higher temperatures, which can be explained as follows: The deactivation occurs above a temperature threshold in the catalyst bed, which is similar for all cases since the autoreduction will be similar (see, for example, ref 62). In contrast, the kinetics of the initiation of the partial oxidation and the reduction of Pd are different since the outer temperature is decisive on the temperature in the catalyst bed. The higher the oven temperature, the faster the buildup of the hot spot and thereby the start of the new period (Figure 10b).

To further improve the signal-to-noise ratio, different procedures for averaging were applied to the QEXAFS data. Averaging with a moving window, including 40 spectra from each second onward, was used with a rectangular (width = 40 s) and a Gaussian (3σ = 40 s) shape. These filters have a rather strong low-pass character along the time axis and can only be applied, when studying regions of the oscillations where the dynamics of the catalyst consist of only low frequencies, respectively, where high time resolution is not required. The rectangular window provides a stronger low-pass character, whereas the Gaussian window has a focus on the middle of the window, yielding a better time resolution with a still reasonable noise reduction. When performing the LCA again on the filtered spectra, the resulting curves representing the amounts of Pd and PdO become very smooth, as shown for the PdO component in Figure S2 in the Supporting Information, where again the data of the FSP catalyst from Figure 1 were used. Because the rectangular window was found to smooth out the transitions between oxidized and reduced states rather strongly, only the Gaussian filter was considered for further investigations. The effect on the extracted EXAFS function is shown in Figure S1 (Supporting Information). Within the smoothed data, it was detected that, in many oscillations, the oxidized and also the reduced state are surprisingly unstable despite the strong low-pass filtering. Oscillations within each state indicate that the surface of the catalyst permanently changes, whereas most changes show up quite regularly with a period of a few seconds. Further analysis was performed in order to investigate these changes.

Because of the suggested more complex progression during the oxidized as well as the reduced state of the oscillation, a PCA

dx.doi.org/10.1021/jp2052294 |J. Phys. Chem. C 2012, 116, 599–609

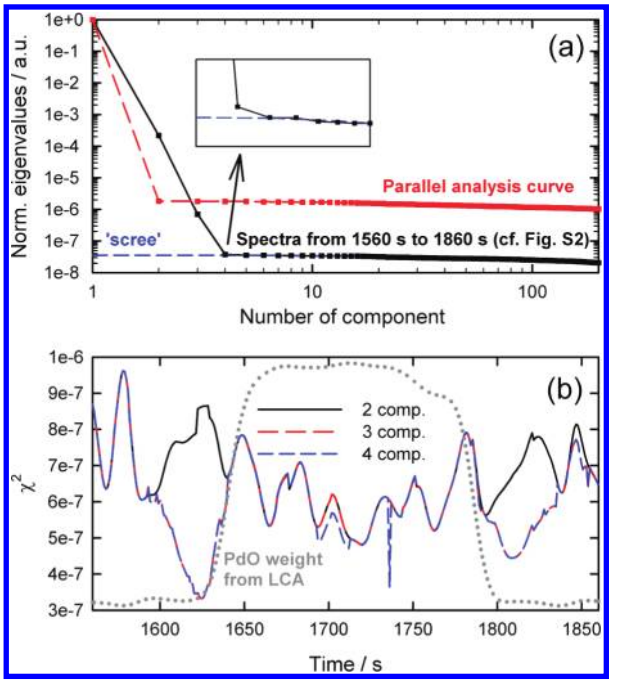

Figure 11. PCA results of one oscillation (data taken from measurements presented in Figure 1) after averaging with a moving Gaussian window with $3\sigma = 40$ spectra: (a) normalized eigenvalues from PCA and applied retention criteria and (b) residuals after reconstructing spectra with various numbers of PCA components plus the qualitative shape of the PdO contribution taken from Figure S2 (Supporting Information) for orientation purposes.

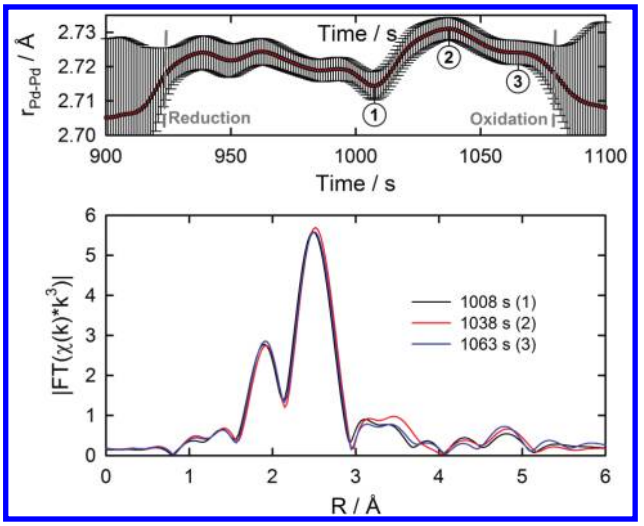

Figure 12. (a) First-neighbor Pd−Pd distance during the reduced state of a selected oscillation after smoothing the spectra in the time dimension with a moving Gaussian window. (b) Selected Fourier transformed Pd K-EXAFS spectra at the positions as marked in (a). Data are taken from the same measurement (FSP catalyst) as used in Figure 11.

was performed with the Gaussian smoothed data to reveal if there are any possible and yet undetermined components. The results for a full oscillation of the Gaussian smoothed data are displayed in Figure 11a. Only two independent components are suggested to be present when applying the parallel analysis factor retaining the decision criterion, which would be the two components already characterized with EXAFS in Figure 8. When applying the scree plot criterion, three or maybe even four independent components seem to appear in the course of the oscillation. To resolve this inconsistency, the spectra of the oscillation were reconstructed with the first 2−4 components yielded by the PCA. The results are shown in Figure 11b, where the mean square displacement of the reconstructed spectra in comparison to the measured spectra is plotted as a function of time. The amount of PdO is sketched schematically as a dotted line without a quantitative scale to give an orientation to which time of the oscillation the data corresponds. Interestingly, a third component improves the reconstruction shortly prior to the oxidation and directly after the reduction, which is strong evidence that there are at least two different states during the reduced state of the catalyst. Including a fourth component improves the reconstruction in the middle of the oxidized state, which is exactly at the turning position seen in the LCA data as a maximum of PdO (cf. Figure 10). However, changes in the QEXAFS spectra are too small to further conclude about the corresponding chemical state.

Further analysis of the EXAFS helps to identify the additional chemical states suggested by the PCA results. Figure 12a shows the next-neighbor Pd distance during the reduced state after applying the 40 s averaging filter to the spectra with the Gaussian window and thereafter performing EXAFS fits by refining the first simulated path of bulk Pd. Thereby, a significant increase in the Pd−Pd distance can be observed prior to the oxidation. With the depicted Fourier transformed spectra in Figure 12b, it is possible to observe that also the higher shells move to higher R values. This behavior can be explained with a lattice expansion due to carbon incorporation into the Pd lattice, which is a well-known phenomenon.[76] For the herein-presented reaction, carbon incorporation was recently predicted by Bychkov et al., who stated that the carbon diffusion proceeds to a maximum C/Pd ratio of ~0.13 before it is oxidized to CO_2.[46] McCaulley et al. performed EXAFS measurements of $PdC_{0.13}$ and compared the spectrum to the one of metallic Pd.[69] The third and fourth shells of $PdC_{0.13}$ are shifted to higher R values similarly as observed in Figure 12b. Furthermore, McCaulley et al. also investigated the XANES and next-neighbor parameters of supported Pd/Al_2O_3 catalysts with hydrogen and carbon incorporation.[75] According to this study, a significant shift of about 2 eV in the position of the XANES peak ($1s \rightarrow 4f$) should be observable in the case of hydrogen incorporation. This was not the case here, as shown in Figure S3 in the Supporting Information, so that the observed lattice expansion is rather explainable with carbon incorporation. However, in a recent study, it was also shown that hydrogen can fill up vacancies depending on the amount of incorporated carbon,[76] which cannot be excluded in this case. It has also to be mentioned that the lattice expansion is not observable in all oscillations, or is present to a lesser extent.

Whenever a lattice expansion is observable, a transition to state 3 (see Figure 12) occurs. Because the Fourier transformation at this instant exhibits an enhanced third shell contribution as typical for bulk fcc Pd, it is most probable that the carbon is removed here, leading to a pure Pd state, which is immediately oxidized. This is also confirmed by the position in energy of the $1s \rightarrow 4f$ XANES transition, which exhibits a minimum at this time and that agrees well with the removal of carbon. This further evidence that poisonous carbonaceous species in the Pd lattice are observable in a short time frame before reoxidation of the catalyst, may be due to the extinction of the total oxidation reaction at the beginning of the catalyst bed (e.g., due to a lower

dx.doi.org/10.1021/jp2052294 |J. Phys. Chem. C 2012, 116, 599–609

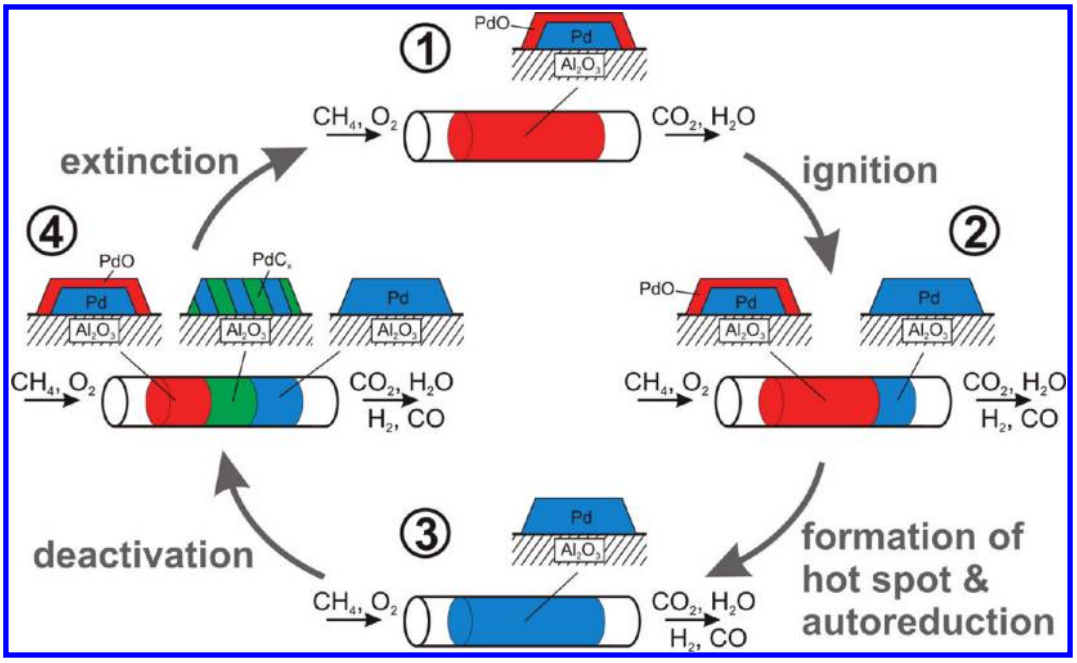

Figure 13. Suggested scheme of the CPO of methane, oscillating on a fixed-bed Pd/Al_2O_3 catalyst, which can be divided into four stages: (1) only total oxidation of methane is observable on the catalyst oxidized over the full length of the catalyst bed, (2) start of reduction at the end of the catalyst bed and start of CPO, (3) formation of a hot spot in the remaining oxidized region leads to self-reduction until the full catalyst bed is reduced, and (4) the surplus oxygen oxidizes the catalyst bed from the beginning with a PdC phase appearing shortly prior to the oxidation because of missing total oxidation. As soon as the full catalyst bed is oxidized again, the CPO no longer occurs and a new cycle begins.

water content, generated by total oxidation, in the gas stream). The appearance of carbon in the Pd particles also agrees well with the presence of a third component in the PCA reconstruction, as shown in Figure 11b. However, it is important to note that the dynamic behavior of the catalyst can also depend on (i) varying surface coverage, (ii) varying particle shapes, (iii) varying carbon/hydrogen incorporation, or (iv) a superposition of several of these processes. Thus, further investigations are required, whereby studies with a combination of complementary techniques, such as presented by Iglesias-Juez et al.[57] and Newton et al.,[74] could help to find out more about such subprocesses of the herein-reported kind during the kinetic oscillations.

4. CONCLUSIONS

The CPO of methane was studied over two different Pd/Al_2O_3 catalysts, providing new insights in the structural changes during the oscillatory behavior of this catalyst system. XANES analysis showed a front of palladium nanoparticle reduction, oscillating through the catalytic fixed bed. This front separated a state where only total oxidation (extinguished state) occurred from a state where the catalytic partial oxidation of methane (ignited state) occurred. These different states are summarized in Figure 13. When the particles are oxidized, complete oxidation is observed (state 1). Upon total oxygen consumption, the catalytic partial oxidation starts, and the catalyst bed is reduced from the end of the reactor to the beginning, where a hot spot in temperature evolves, leading to a transition state, where the first part of the catalyst is still in an oxidized state (state 2). Because of the nonlinear exponential Arrhenius term, a self-acceleration of the total oxidation reaction and a further increase of the temperature in the catalyst bed occurred until the autoreduction temperature of Pd is reached and the palladium is fully reduced (state 3). This causes a drop in activity of methane oxidation. The partial oxidation of methane extinguishes, and correspondingly, the catalyst bed reoxidizes from the beginning of the catalyst bed to its end (state 4). QEXAFS data analysis of a wide range of parameter sets showed that at least three significant species have to be taken into account to reproduce the QEXAFS spectra during oscillation cycles. Furthermore, prior to the reoxidation, the higher shells become more characteristic of bulk Pd metal, probably due to desorption of the reactants, before a lattice expansion occurs, which was attributed to carbon incorporation into the lattice (state 4, Figure 13). The frequency of the oscillations increased with increasing O_2/CH_4 ratio, while sintering of the Pd particles during 35 h on stream could be observed, resulting in a slightly lower oscillation frequency. This study demonstrates that QEXAFS in combination with appropriate analysis procedures is a powerful tool for revealing independent components in the course of a reaction and yields new insight into fast and highly dynamic catalytic processes.

■ ASSOCIATED CONTENT

Supporting Information. The extracted EXAFS functions after applying various filter techniques to the QEXAFS spectra (Figure S1) and the intensity, positions in energy, of the XANES peaks as a function of time for an exemplary measurement during oscillations (Figure S2) are found in the Supporting Information. This material is available free of charge via the Internet at http://pubs.acs.org.

■ AUTHOR INFORMATION

Corresponding Author

*E-mail: j.stoetzel@uni-wuppertal.de (J.S.), grunwaldt@kit.edu (J.-D.G.).

■ ACKNOWLEDGMENT

We thank Matthias Beier (Technical University of Denmark) for his help during the beamtime. The Swiss Light Source (SLS), the Danish council for strategic research (DSF), and Danscatt are acknowledged for providing beamtime and financial support.

■ REFERENCES

(1) Ertl, G.; Norton, P. R.; Rüstig, J. *Phys. Rev. Lett.* **1982**, *49*, 177.
(2) Eiswirth, M.; Ertl, G. *Surf. Sci.* **1986**, *177*, 90.
(3) Schüth, F.; Henry, B. E.; Schmidt, L. D. *Adv. Catal.* **1993**, *39*, 51.
(4) Slinko, M. M.; Jaeger, N. I. *Oscillatory Heterogeneous Catalytic Systems*; Elsevier: Amsterdam, 1994.
(5) Imbihl, R.; Ertl, G. *Chem. Rev.* **1995**, *95*, 597.
(6) Gruyters, M.; King, D. A. *J. Chem. Soc., Faraday Trans.* **1997**, *93*, 2947.
(7) Imbihl, R. *Handbook of Surface Science*; Elsevier: Amsterdam, 2008; Chapter 9.
(8) Reuter, K.; Scheffler, M. *Phys. Rev. B* **2003**, *68*, 045407.
(9) Zhdanov, V. P. *Surf. Sci.* **2002**, *500*, 966.
(10) Johánek, V.; Laurin, M.; Grant, A. W.; Kasemo, B.; Henry, C. R.; Libuda, J. *Science* **2004**, *304*, 1639.
(11) Zhdanov, V. P. *Phys. Rev. E* **1999**, *60*, 7554.
(12) Sales, B. C.; Turner, J. E.; Marple, M. B. *Surf. Sci.* **1982**, *114*, 381.
(13) Collins, N. A.; Sundaresan, S.; Chabal, Y. J. *Surf. Sci.* **1987**, *180*, 136.
(14) Hendriksen, B. L. M.; Ackermann, M. D.; van Rijn, R.; Stoltz, D.; Popa, I.; Balmes, O.; Resta, A.; Wermeille, D.; Felici, R.; Ferrer, S.; Frenken, J. W. M. *Nat. Chem.* **2010**, *2*, 730.
(15) Thomas, J. M. *Angew. Chem., Int. Ed.* **1999**, *38*, 3588.
(16) Grunwaldt, J.-D.; Clausen, B. S. *Top. Catal.* **2002**, *18*, 37.
(17) Topsøe, H. *J. Catal.* **2003**, *216*, 155.
(18) Baranes, M. A. *Catal. Today* **2005**, *100*, 71.
(19) Hansen, P. L.; Wagner, J. B.; Helveg, S.; Rostrup-Nielsen, J. R.; Clausen, B. S.; Topsøe, H. *Science* **2002**, *295*, 2053.
(20) Clausen, B. S.; Topsøe, H.; Frahm, R. *Adv. Catal.* **1998**, *42*, 315.
(21) Grunwaldt, J.-D.; Molenbroek, A. M.; Topsøe, N.-Y.; Topsøe, H.; Clausen, B. S. *J. Catal.* **2000**, *194*, 452.
(22) Jentys, A. *Phys. Chem. Chem. Phys.* **1999**, *1*, 4059.
(23) Fernandez-Garcia, M. *Catal. Rev. Sci. Eng.* **2002**, *44*, 59.
(24) Newton, M. A.; Dent, A. J.; Evans, J. *Chem. Soc. Rev.* **2002**, *31*, 83.
(25) Ressler, T.; Jentoft, R. E.; Wienold, J.; Girgsdies, F.; Neisius, T.; Timpe, O. *Nucl. Instrum. Methods Phys. Res., Sect. B* **2003**, *200*, 165.
(26) Grunwaldt, J.-D.; Caravati, M.; Hannemann, S.; Baiker, A. *Phys. Chem. Chem. Phys.* **2004**, *6*, 3037.
(27) Bare, S. R.; Ressler, T. *Adv. Catal.* **2009**, *52*, 339.
(28) Grunwaldt, J.-D. *J. Phys. Conf. Ser.* **2009**, *190*, 012151.
(29) Ressler, T.; Hagelstein, M.; Hatje, U.; Metz, W. *J. Phys. Chem. B* **1997**, *101*, 6680–6687.
(30) Kimmerle, B.; Baiker, A.; Grunwaldt, J.-D. *Phys. Chem. Chem. Phys.* **2010**, *12*, 2288–2291.
(31) Singh, J.; Nachtegaal, M.; Alayon, E. M. C.; Stötzel, J.; van Bokhoven, J. A. *ChemCatChem* **2010**, *2*, 653.
(32) Frahm, R. *Nucl. Instrum. Methods Phys. Res., Sect. A* **1988**, *270*, 578.
(33) Frahm, R. *Rev. Sci. Instrum.* **1989**, *60*, 2515.
(34) Reimann, S.; Stötzel, J.; Frahm, R.; Kleist, W.; Grunwaldt, J.-D.; Baiker, A. *J. Am. Chem. Soc.* **2011**, *133*, 3921–3930.
(35) Grunwaldt, J.-D.; Beier, M.; Kimmerle, B.; Baiker, A.; Nachtegaal, M.; Griesebock, B.; Lützenkirchen-Hecht, D.; Stötzel, J.; Frahm, R. *Phys. Chem. Chem. Phys.* **2009**, *11*, 8779–8789.
(36) Basini, L.; Aasberg-Petersen, K.; Guarinoni, A.; Ostberg, M. *Catal. Today* **2001**, *64*, 9–20.
(37) Recupero, V.; Pino, L.; Di Leonardo, R.; Lagana, M.; Maggio, G. *J. Power Sources* **1998**, *71*, 208–214.
(38) Bychkov, V. Y.; Tyulenin, Y. P.; Korchak, V. N.; Aptekar, E. L. *Appl. Catal., A* **2006**, *304*, 21–29.
(39) Bychkov, V. Y.; Tyulenin, Y. P.; Slinko, M. M.; Korchal, V. N. *Appl. Catal., A* **2007**, *321*, 180–189.
(40) König, D.; Weber, W. H.; Poindexter, B. D.; Mcbride, J. R.; Graham, G. W.; Otto, K. *Catal. Lett.* **1994**, *29*, 329.
(41) Ozkan, U. S.; Kumthekar, M. W.; Karakas, G. *J. Catal.* **1997**, *171*, 67–76.
(42) Graham, G. W.; König, D.; Poindexter, B. D.; Remillard, J. T.; Weber, W. H. *Top. Catal.* **1999**, *8*, 35–43.
(43) Deng, Y.; Nevell, T. G. *J. Mol. Catal. A* **1999**, *142*, 51–60.
(44) Zhang, X.; Lee, C. S.-M.; Mingos, D. M. P.; Hayward, D. O. *Appl. Catal.* **2003**, *240*, 183–197.
(45) Zhang, X.; Lee, C. D.-M.; Hayward, D. O.; Mingos, D. M. P. *Catal. Today* **2005**, *105*, 283–294.
(46) Bychkov, V. Yu.; Tyulenin, Yu. P.; Slinko, M. M.; Shashkin, D. P.; Korchak, V. N. *J. Catal.* **2009**, *267*, 181.
(47) Strobel, R.; Grunwaldt, J.-D.; Camenzind, A.; Pratsinis, S. E.; Baiker, A. *Catal. Lett.* **2005**, *104*, 9.
(48) Hannemann, S.; Grunwaldt, J.-D.; Lienemann, P.; Gunther, D.; Krumeich, F.; Pratsinis, S. E.; Baiker, A. *Appl. Catal., A* **2007**, *316*, 226.
(49) Frahm, R.; Nachtegaal, M.; Stötzel, J.; Harfouche, M.; van Bokhoven, J. A.; Grunwaldt, J.-D. *AIP Conf. Proc.* **2010**, *1234*, 251–255.
(50) Frahm, R.; Richwin, M.; Lützenkirchen-Hecht, D. *Phys. Scr.* **2005**, *T115*, 974–976.
(51) Stötzel, J.; Lützenkirchen-Hecht, D.; Fonda, E.; de Oliveira, N.; Briois, V.; Frahm, R. *Rev. Sci. Instrum.* **2008**, *79*, 083107.
(52) Stötzel, J.; Lützenkirchen-Hecht, D.; Frahm, R. *J. Synchrotron Radiat.* **2011**, *18*, 165–175.
(53) Newville, M. *J. Synchrotron Radiat.* **2001**, *8*, 322–324.
(54) Zabinsky, S. I.; Rehr, J. J.; Ankudinov, A.; Albers, R. C.; Eller, M. J. *Phys. Rev. B* **1995**, *52*, 2995.
(55) Horn, J. L. *Psychometrika* **1965**, *32*, 179–185.
(56) Cattell, R. B. *Multivar. Behav. Res.* **1966**, *1*, 245–276.
(57) Iglesias-Juez, A.; Kubacka, A.; Fernández-García, M.; Di Michiel, M.; Newton, M. A. *J. Am. Chem. Soc.* **2011**, *133*, 4484.
(58) Grunwaldt, J.-D.; Schroer, C. G. *Chem. Soc. Rev.* **2010**, *39*, 4741.
(59) Kimmerle, B.; Grunwaldt, J.-D.; Baiker, A.; Glatzel, P.; Boye, P.; Stephan, S.; Schroer, C. G. *J. Phys. Chem. C* **2009**, *113*, 3037.
(60) Grunwaldt, J.-D.; Kimmerle, B.; Baiker, A.; Boye, P.; Schroer, C. G.; Glatzel, P.; Borca, C. N.; Beckmann, F. *Catal. Today* **2009**, *145*, 267.
(61) Kimmerle, B.; Haider, P.; Grunwaldt, J.-D.; Baiker, A.; Boye, P.; Schroer, C. G. *Appl. Catal., A* **2009**, *353*, 36.
(62) Grunwaldt, J.-D.; van Vegten, N.; Baiker, A. *Chem. Commun.* **2007**, 4635.
(63) Hartmann, M.; Maier, L.; Deutschmann, O. *Appl. Catal., A* **2011**, *391*, 144–152.
(64) Dalle Nogare, D.; Degenstein, N. J.; Horn, R.; Canu, P.; Schmidt, L. D. *J. Catal.* **2011**, *277*, 134–148.
(65) Grunwaldt, J.-D.; Molenbroek, A. M.; Topsøe, N.-Y.; Topsøe, H.; Clausen, B. S. *J. Catal.* **2000**, *194*, 452.
(66) Lopez, N.; Nørskov, J. K.; Janssens, T. V. W.; Calsson, A.; Puig-Molina, A.; Clausen, B. S.; Grunwaldt, J.-D. *J. Catal.* **2004**, *225*, 86.
(67) Hansen, P. L.; Wagner, J. B.; Helveg, S.; Rostrup-Nielsen, J. R.; Clausen, B. S.; Topsøe, H. *Science* **2002**, *295*, 2053.
(68) Grunwaldt, J.-D.; Caravati, M.; Baiker, A. *J. Phys. Chem. B* **2006**, *110*, 25586.
(69) McCaulley, J. A. *Phys. Rev. B* **1993**, *47*, 4873.
(70) Mackay, A. L. *Acta Crystallogr.* **1962**, *15*, 916.
(71) Yevick, A.; Frenkel, A. *Phys. Rev. B* **2010**, *81*, 115451.
(72) Clausen, B. S.; Nørskov, J. K. *Top. Catal.* **2000**, *10*, 221–230.
(73) Demoulin, O.; Le Clef, B.; Navez, M.; Ruiz, P. *Appl. Catal., A* **2008**, *344*, 1–9.
(74) Newton, M. A.; Di Michiel, M.; Kubacka, A.; Fernández-García, M. *J. Am. Chem. Soc.* **2010**, *132*, 4540.
(75) McCaulley, J. A. *J. Phys. Chem.* **1993**, *97*, 10372.
(76) Vogel, W. *J. Phys. Chem. C* **2011**, *115*, 1506.